Plasmonic Metamaterials Absorbers Design Based on XGBoost and LightGBM Algorithms

Leilei Gu
South China Normal University
Shusheng Xie
South China Normal University
Ying Zhang
South China Normal University
Yule Huang
South China Normal University
Yaojun He
South China Normal University
Hongzhan Liu
South China Normal University
Zhongchao Wei
South China Normal University
Jian Ping Guo (guojpgz@163.com)
South China Normal University https://orcid.org/0000-0001-7211-7409

Research Article

Keywords: Metamaterials, Inverse design, LightGBM, XGBoost, Refractive index

Posted Date: March 24th, 2022

DOI: https://doi.org/10.21203/rs.3.rs-1460964/v1

Abstract

The emergence of metamaterials has brought a revolutionary way to manipulate the behavior of light on the nanoscale. However, there are still many problems in design process, such as time-consuming, many-to-one mapping, etc. Here, we demonstrate the forward and inverse design of plasmonic metamaterials absorbers based on Light gradient boosting machine (LightGBM) and Extreme Gradient Boosting (XGBoost). The inverse framework can use the input reflective index value to design the metamaterial parameter structure. The experimental results show that XGBoost has better performance in forward and inverse design (Forward-R^2: 0.956; Inverse-R^2: 0.967). The framework is suitable for designing metamaterials on demand, and it can be used in zoom imaging, metamaterials absorbers, metamaterials filters and other fields.

1. Introduction

One of the nanophotonics research targets is to get a better understand on optical phenomena at the nanometer scale. Among them, the use of metamaterials to manipulate and control the interaction between light and matter at the micro and nano scale has attracted extensive attention of researchers [1, 2]. In recent years, different kinds of devices based on metamaterials have been designed and demonstrated, such as absorbing materials [3–5], holographic imaging [6], multiparameter adjustable thermal diodes [7], radome [8]. In special, Deng et al. provided an advanced metasurface information steganography technology. Its arbitrary polarization angle image multiplexing and hiding function can stimulate a wave of new optical information devices [9]. Wang et al. demonstrated the design of all-in-one polarizer suitable for function at an arbitrary position on the Poincaré sphere, which is a universal design of all-dielectric metasurfaces to achieve perfect APCD [10]. Qin et al. improved the focusing efficiency of metalens by heating, increasing voltage and changing materials, which has reference significance for the study of optical storage, communication and imaging [11, 12]. In these studies, the design of metamaterials has become a popular study topic.

In order to obtain the structure, composition, and geometric size of the device with the desired optical response, the general method is to design a specific model based on experience, and then continuously revise it until a satisfactory result is finally obtained, which is a time-consuming task that requires the designer to have extensive experience. Additionally, the design process relies strongly on empirical reasoning or trial and error, which is inefficient and often ineffective, especially when the problem is highly nonlinear. Therefore, it is necessary to find a new approach to simplify or even replace traditional design methods. Some pioneering works have been reported during last few years. Peurifoy et al. successfully realized the prediction of the scattering cross section by using the distance between the multi-layer core-shell nanoparticle as the input of the deep neural network (DNN) model and the scattering cross section as the outputs [13]. In addition to the application in forward design, Liu et al. applied neural network in the inverse design for SiO2 and Si3N4 multilayer structures, in which the thickness of each layer and the transmission spectrum are established mapping relations [14]. But most of these works lack the performance metrics of experimental results and fail to combine forward design and inverse design.

Recently, ensemble learning has played an important role in promoting interdisciplinary integration, and has been successfully applied in meteorology [15], physics [16], and biology [17]. The mapping relationship between data is obtained by imitating human learning methods, and is divided into two types: regression and classification according to the purpose of the research. As a new type of experience model Boosting algorithm in ensemble learning, it is widely used in classification and regression.

To solve these challenges, we proposed the forward and inverse design of metamaterial absorbers based on ensemble learning (XGBoost, LightGBM) algorithms. The six structures ($x1…x6$) parameters are taken as the input, and the fifteen refractive indexes ($y1…y15$) is taken as the output to establish the forward design model while the inverse design model is the opposite. It shows that the excellent generalization ability of the inverse design model. In the forward design, the average regression coefficients of XGBoost and LightGBM are 0.956 and 0.876, respectively. In the inverse design, their R2 are 0.907 and 0.967, respectively. The establishment of inverse design not only speeds up the design of metamaterial structures, but also reduces error rates. Meanwhile, the input and output of the framework can be changed according to the requirements of the design. Hence, our study may provide an approach for the design of nanophotonic functional devices.

2. Materials And Methods

2.1. Data preparation

In this article, we try to design a metamaterial absorber working in visible and near-infrared bands by using ensemble learning method. The proposed metamaterial has periodic structure whose construction minimum unit consists of three layers (Fig. 1). The top and bottom layers are both silver materials, while the top layer is an array of silver particles, and the bottom layer is a continuous silver film. A thin dielectric layer is selected as the intermediate layer to separate the two metal layers. The structure is manufactured under ideal conditions. The metamaterial studied in this paper has six structural parameters, and the structural parameters and materials are marked in the figure. Simulation was carried out through the finite-difference time-domain (FDTD) method with the commercial software Lumerical FDTD Solutions. The x and y directions are periodic boundary conditions, and the z direction is PML boundary conditions. By sweep the values of structural parameters, the refractive index of different parameters is generated. Collect the refractive index of all structural parameters under FDTD simulation to form a data set.

2.2. Forward and inverse design framework

The process of predicting refractive index by forward design framework is shown in Fig. 2. Six structural parameters in the metamaterial are input to the model, and the output is refractive index. The ratio of the training set to the testing set is 8:2. The upper part of the framework is the training part. Its essence is to obtain the objective function by training the mapping relationship between structural parameters and reflectivity. Furthermore, the input of the test set is imported into the objective function to obtain the calculated value of reflectivity. Homoplastically, the inverse design model is based on the optimized

parameters of the forward model. (Fig. 3). The refractive spectrum is input and the structural parameters are output. Consequently, by changing the values of different refractive spectrum, a new metamaterial structure can be designed.

2.3 Machine learning approach

The derivation process of the two models is shown in the Appendix. For ensemble learning algorithm, parameter setting is the key to improve model prediction performance. Under the same data set, the optimal parameters are obtained through orderly debugging parameters. For LightGBM and XGBoost Model, the optimized parameters and their default values are shown in Table 1, 2. The time-consuming for each forward design of the model is shown in Appendix tables S3, S4.

Table 1
LightGBM model core parameters.

Parameters	Meaning	Values	Effect
num_boost_round	The number of iterations	5000	Improve accuracy
bagging_fraction	The ratio of data used in each iteration.	1	Prevent overfitting
feature_fraction	Randomly select certain parameters to build the tree in the iteration	1	Reduce overfitting
bagging_freq	Bagging times	5	Prevent overfitting
learning_rate	Converge the objective function to the minimum	0.01	Improve accuracy
num_leaves	Number of leaf nodes	31	Prevent overfitting
max_depth	Maximum depth of tree	50	Reduce overfitting
verbose	Control the level of approach verbosity	10	Increase efficiency

Table 2
XGBoost model core parameters.

Parameters	Meaning	Values	Effect
num_boost_round	The number of iterations	3000	Improve accuracy
colsample_bytree	Control the proportion of the number of randomly sampled columns in each tree	1	Improve accuracy
learning_rate	Leaning rate	0.001	Prevent overfitting
subsample	The sampling rate of per tree	0.9	Prevent overfitting
lambda	L2 regularization	0	Improve generalization ability
alpha	L2 regularization	1	Prevent overfitting

3. Results And Discussion

3.1 Forward Design

After the feature value are linearly normalized, the data sets are shuffled (Break down the contingency of data arrangement and prevent over-fitting). The loss functions of the training and testing set of the two models are shown in Fig. 4. The setting of the training epochs size determines the fitting procedure of the model, and the loss value of the training set generally decreases as the training epochs size increases. Whereas, after the loss value drops to a certain degree, if the training is continued, the model will be overfitting due to the loss increasing process. On the contrary, too small epochs size will result in underfitting [17]. Hence, the appropriate training step length is very important for forward and inverse design. It can be seen that the LightGBM model converges quickly in the first 500 training epochs. In the subsequent training, the convergence rate gradually decreased and reached stability after 2000 epochs, and the final optimal training step size was 5000. Its loss values for training and testing are 4.0E-04 and 1.113E-02, respectively. The XGBoost also converges quickly in the first 500 epochs, and gradually stabilizes after 1000 epochs of training. The optimal training epochs size is 3000. It has a stable training loss value of 9.4E-04 and a stable testing loss value of 1.62E-03. The loss values of other parameters are shown in appendix fig. S2, S3.

Figure 4. Model convergence of XGBoost and LightGBM (Parameter y1).

The predicted value and target value of forward design are shown in Fig. 5, 6 ($x1 \sim x6$). The XGBoost and LightGBM predicted of reflectivity index shown in appendix fig. S4, S5 ($x7 \sim x15$). The degree of deviation between the target value and the predicted value under the standard line, and the vertical distance from the dotted line indicates the error of the prediction. From the distribution of the value, it can be concluded that the deviation between the true value and the predicted value is small. The fitting effect at the last few parameters index is almost the same as the true value. In the prediction of 15 *y* datasets, the overall prediction accuracy of XGBoost was better compared to LightGBM.

Figure 5. The distribution of predicted and true values in the test set (F-XGBoost).

Figure 6. The distribution of predicted and true values in the test set (F-LightGBM).

The distribution of the predicted and true values of the refractive index in the test set is shown in Fig. 7. The three-dimensional structure makes it easier to see the distribution of the true value and the predicted value. Although there is a certain difference in the size of the value, all index is distributed on an inclined plane. Compared with the LightGBM model, the XGBoost model predictive value has a smaller degree of dispersion.

Figure 7. The distribution of the predicted value and target value of *y* refractive index in the test set (a: F-XGBoost, b: F-LightGBM).

In order to evaluate the predictive performance of algorithms, four standard metrics were selected: Root Mean Square Error (RMSE) [18], Mean absolute error (MAE) [19], Pearson correlation (R) [20], and Regression coefficients (R2) [21].

The error between the predicted value of the prediction model and the simulated value of FDTD reflects the resilience for new data sets of the model. Compared with previous work, we have scrambled the data to prevent accidental problems. Comparing the predicted value curves of FDTD and XGBoost in the test set, it is observed that the two curves almost completely overlap (parameters 1 to 6), and the prediction curves of other parameters have small errors in some areas of the FDTD simulation curve (Fig. 8, 9).

Compared with the LightGBM model, the performance of XGBoost is more stable, and the predicted value is closer to the simulated value (Appendix fig. S6, S7).

Figure 8. Curve of FDTD simulation value and model prediction value(F-XGBoost).

Figure 9. Curve of FDTD simulation value and model prediction value(F-LightGBM).

Performance metrics is an important evaluation index to measure the generalization ability of the model. The Pearson correlation coefficient curve is stable (0.90 ~ 1.00). It shows that the structural parameters have a strong correlation with reflectivity value. The overall reflectivity prediction accuracy of XGBoost is better than that of LightGBM, with 13 refractive indexes accuracy above 0.950. The value of RMSE and MAE can accurately reflect the error size of the model. As can be seen from the distribution of values in the figure, the minimum values of RMSE and MAE for the LightGBM model are 0.0353 and 0.0217, respectively. For XGBoost, the RMSE and MAE minimum vales are 0.01 and 0.0062, respectively. XGBoost model has a better fitting for data. (Fig. 10). This related to the different decision tree growth strategies of the two algorithms. XGBoost uses the Level-wise strategy to learn features more efficiently than Leaf-wise. The predictive performance of test sets at different proportions are shown in appendix table S5.

Figure 10. Model performance metrics (a: F-XGBoost, b: F-LightGBM).

3.2 Inverse Design

Figure 11. Distribution of predicted and true values in test data (I-XGBoost).
(a) parameters $x1$. (b) parameters $x2$. (c) parameters $x3$. (d) parameters $x4$

In the inverse design, the refractive spectrum is input into the model to predict the structural parameters. We demonstrate predictive for four main structural parameters. The models show good performance, and the LightGBM model is more stable and accurate in parameters $x1$ compared with XGBoost, while parameter $x2$ is the opposite. There are small errors in structural parameters $x3$ and $x4$. Among the

deviations between the overall predicted value and the true value. The LightGBM model structure has better resilience for new datasets. (Fig. 11).

Select the first 20 data in the test set for observation and comparison. In the prediction of structural parameters *x*1 and *x*3, there are only two deviations between the predicted value and the true value. There were three deviations in the *x*4 prediction. The predicted value of the structural parameter *x*2 is completely consistent with the true value (Fig. 12). The model has achieved the target effect in the design of structural parameters and has potential for the design of new metamaterials. Then the design of the metamaterial structure is more diverse.

Figure 12. The predicted and target values of six structural parameters in inverse design (I-LightGBM).

In the inverse design performance metrics value. The maximum RMSE value is 0.006 and the minimum value is 0.004 (LightGBM). The minimum RMSE value of XGBoost reached 0.002, which is even smaller. It shows that the error between the true value and the predicted value is small. In the prediction of structural parameters *x*1 and *x*2, the optimal regression coefficients (R^2) are 0.997 (LightGBM) and 0.999 (XGBoost). The predictions of structural parameters *x*3 and *x*4 also have good accuracy (Table 3). From the graphical distribution of the two models, the overall performance of XGBoost is more stable (Fig. 13).

Table 3. Evaluation index of model in inverse design.

Algorithm	Parameter	RMSE	MAE	R	R^2
LightGBM	*x*1	0.003	0.003	1.000	0.997
	*x*2	0.006	0.004	0.996	0.989
	*x*3	0.006	0.005	0.944	0.738
	*x*4	0.004	0.003	0.988	0.902
XGBoost	*x*1	0.002	0.001	1.000	0.999
	*x*2	0.004	0.002	0.997	0.993
	*x*3	0.002	0.001	0.970	0.934
	*x*4	0.003	0.001	0.982	0.941

Figure 13. Comparison of XGBoost and LightGBM performance metrics.

(Lower left: R; Upper left: RMSE; Lower right: R^2; Upper right: MAE)

Compared with the deep learning inverse design method in the reference, we added more performance indicators to evaluate the model, and verified the performance of the model through indicators. The two algorithm models achieve smaller errors and higher accuracy. Therefore, XGBoost and LightGBM model have a supporting research role in metamaterial design.

4. Conclusion

In this paper, we demonstrate the application of the LightGBM and XGBoost algorithms in the forward and inverse design of metamaterials. The forward design simulation software simulates the refractive index. The designed inverse framework can use the input reflectivity value to design the metamaterial parameter structure, which greatly reduces the time required to solve the inverse problem, and generates new metamaterial structures through flexible combinations. The experimental results show that the forward and inverse LightGBM average regression coefficient values are 0.876 and 0.907, respectively. Compared with LightGBM, XGBoost has better performance in forward and inverse design (F-R^2: 0.956; I-R^2: 0.967). Not only the performance metrics has been greatly improved, but the two models have small requirements for the equipment. This provides a good tool for the aid of FDTD solutions simulation experiment. Our study opens a new avenue to realize the prediction of metamaterial reflectivity and structure parameter, and the LightGBM can also inspire the inverse design of other metamaterials and photonics. Nevertheless, although the predicted fitting value has reached a high accuracy, it is limited to the study of the structural parameters and reflectivity of specific materials. Accordingly, the next step is to add material characteristics to the input dimensions to broaden the design of metamaterials.

Declarations

Funding

This work has been supported by National Natural Science Foundation of China (Grant No. 61774062, No. 61875057 and No.11674109); Natural Science Foundation of Guangdong Province, China (Grant No. 2021A1515010352, NO. 2021A1515012652);

Conflicts of interest

The authors declare that they have no known competing financial interests or personal relationships that could have appeared to influence the work reported in this paper.

Availability of data and material

The datasets generated during and/or analysed during the current study are not publicly available due to needs for the next study but are available from the corresponding author on reasonable request.

Authors' contributions

All authors contributed to the study conception and design. Material preparation, data collection and analysis were performed by Leilei Gu, Shusheng Xie and Ying Zhang. The first draft of the manuscript was written by Leilei Gu and all authors commented on previous versions of the manuscript. All authors read and approved the final manuscript.

Ethics approval

This is an observational study. The XYZ Research Ethics Committee has confirmed that no ethical approval is required.

Consent to participate

Informed consent was obtained from all individual participants included in the study.

Consent for publication

The authors affirm that human research participants provided informed consent for publication of the images in Figure.

References

1. Hou, Z., T. Tang, J. Shen, C. Li, and F. Li (2020)Nanoscale research letters 15 1-8

2. Zhao, J.-X., J.-L. Song, Y. Zhou, Y.-C. Liu, and J.-H. Zhou (2020)Chinese Physics Letters 37 064204

3. Chen, P., X. Kong, J. Han, W. Wang, K. Han, H. Ma, L. Zhao, and X. Shen (2021)Chinese Physics Letters 38 027801

4. Liu, Y.-N., X.-L. Weng, P. Zhang, W.-X. Li, Y. Gong, L. Zhang, T.-C. Han, P.-H. Zhou, and L.-J. Deng (2021)Chinese Physics Letters 38 034201

5. Hewlett, S. and A. Mock (2017)Plasmonics 12 419-425

6. Hunt, J., J. Gollub, T. Driscoll, G. Lipworth, A. Mrozack, M.S. Reynolds, D.J. Brady, and D.R. Smith (2014)JOSA A 31 2109-2119

7. Toyin, O.R., W. Ge, and L. Gao (2021)Chinese Physics Letters 38 016801

8. Narayan, S., G. Gulati, B. Sangeetha, and R.U. Nair (2018)IEEE Transactions on Antennas and Propagation 66 4695-4707

9. Deng, Z.L., Q.A. Tu, Y. Wang, Z.Q. Wang, T. Shi, Z. Feng, X.C. Qiao, G.P. Wang, S. Xiao, and X. Li (2021)Adv. Mater. 33 2103472

10. Wang, S., Z.-L. Deng, Y. Wang, Q. Zhou, X. Wang, Y. Cao, B.-O. Guan, S. Xiao, and X. Li (2021)Light: Science & Applications 10 1-9

11. Qin, S., H. Huang, K. Jie, S. Zeng, L. Chen, H. Liu, J. Guo, H. Meng, F. Wang, and X. Yang (2021)Nanomaterials 11 2023

12. Qin, S., N. Xu, H. Huang, K. Jie, H. Liu, J. Guo, H. Meng, F. Wang, X. Yang, and Z. Wei (2021)Optics Express 29 7925-7934

13. Peurifoy, J., Y. Shen, L. Jing, Y. Yang, F. Cano-Renteria, B.G. DeLacy, J.D. Joannopoulos, M. Tegmark, and M. Soljačić (2018)Sci. Adv. 4 4206

14. Liu, D., Y. Tan, E. Khoram, and Z. Yu (2018)Acs Photonics 5 1365-1369

15. Zhang, X.x., L.l. Gu, H. Chen, and G.z. Jia (2020)Concurrency and Computation: Practice and Experience 32 5921

16. Deng, T. and G.-z. Jia (2020)Molecular Physics 118 1600754

17. Deng, T., F.-h. Liu, and G.-z. Jia (2020)Molecular Physics 118 1652367

18. Chai, T. and R.R. Draxler (2014)Geoscientific Model Development Discussions 7 1525-1534

19. Willmott, C.J. and K. Matsuura (2005)Climate research 30 79-82

20. Jebli, I., F.-Z. Belouadha, M.I. Kabbaj, and A. Tilioua (2021)Energy 224 120109

21. Clogg, C.C., E. Petkova, and A. Haritou (1995)Am. J. Sociol. 100 1261-1293

Figures

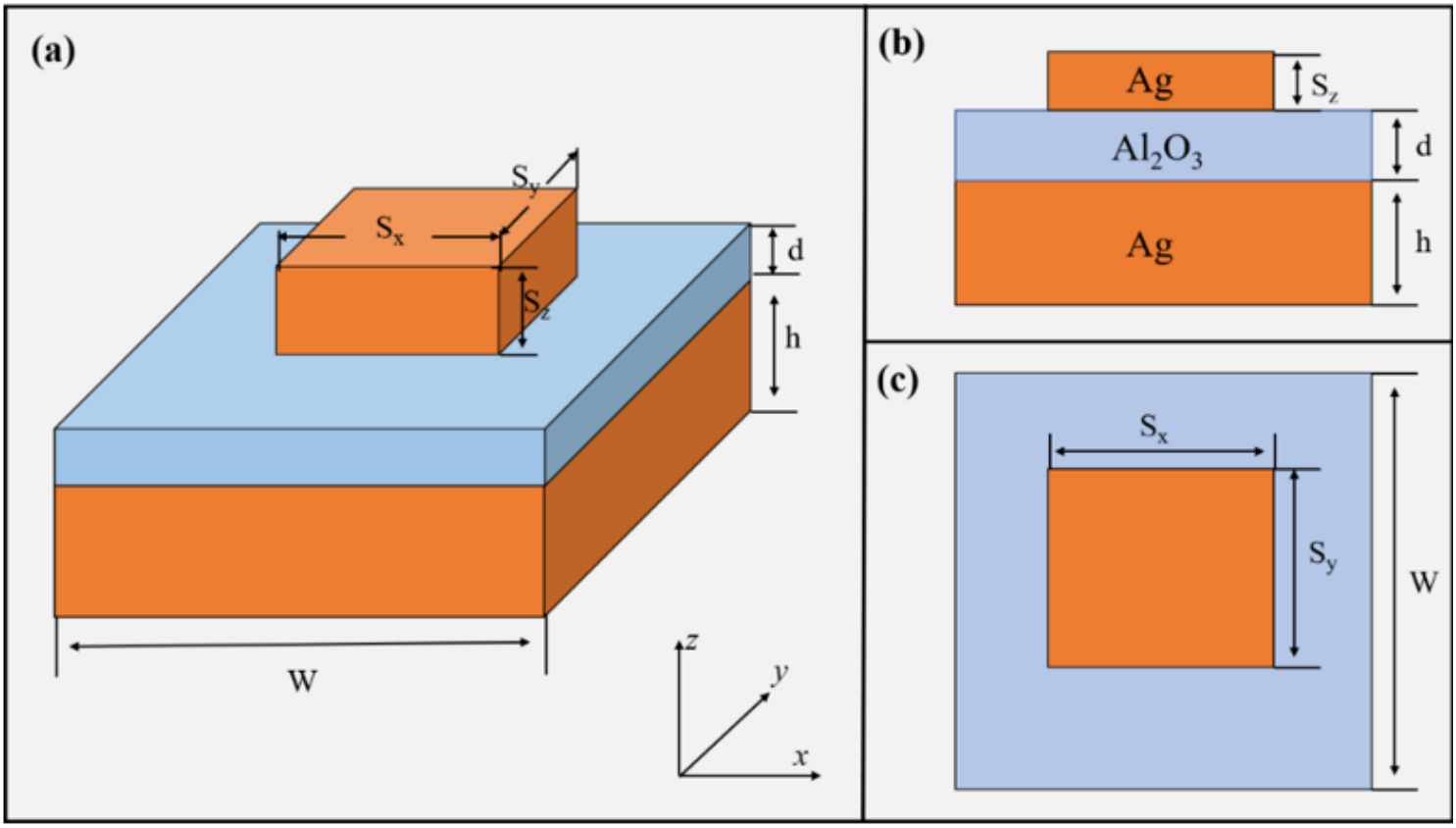

Figure 1

Geometry and parameter of the structures studied in this paper.

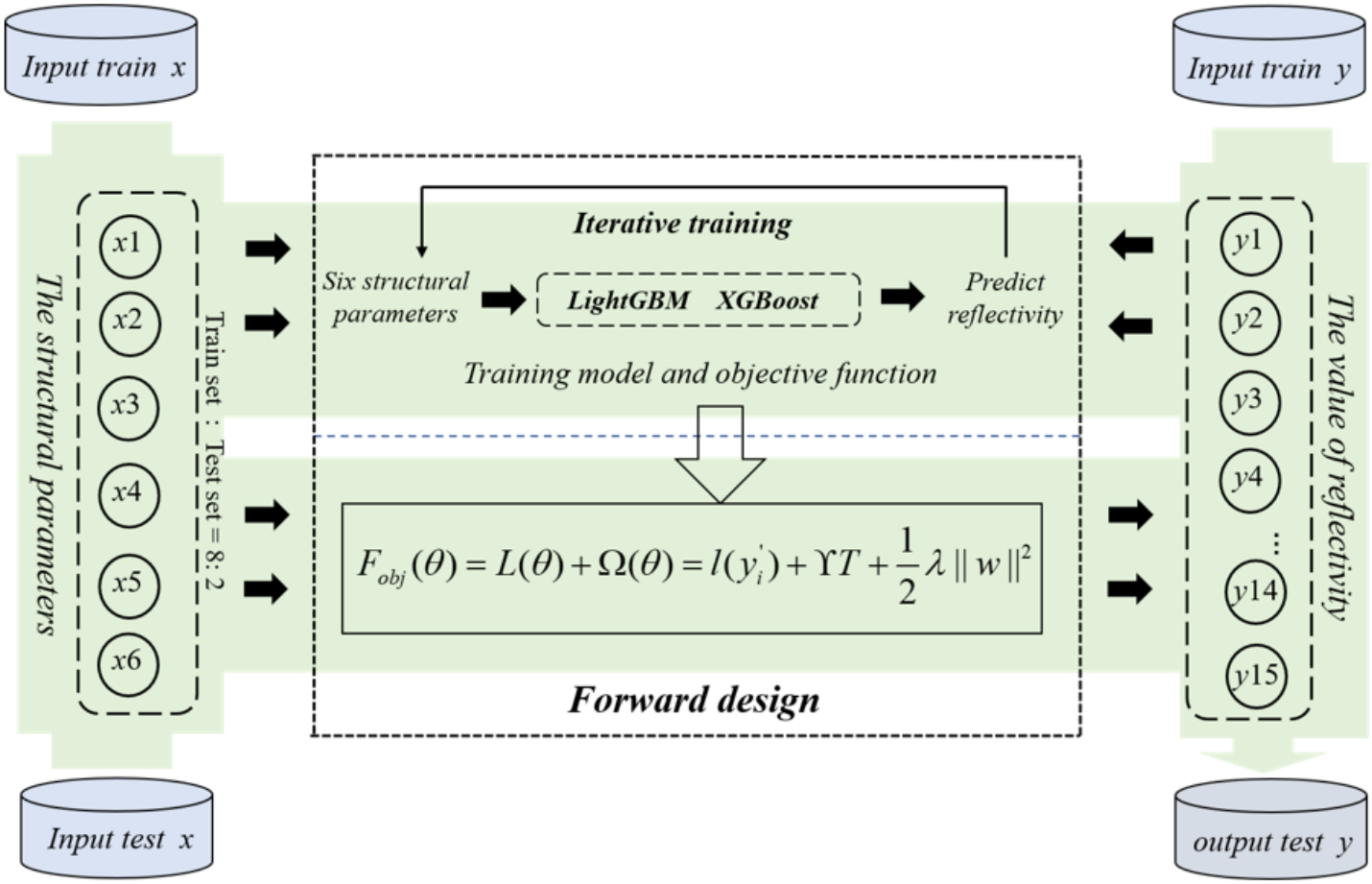

Figure 2

The process of predicting refractive index by forward design framework.

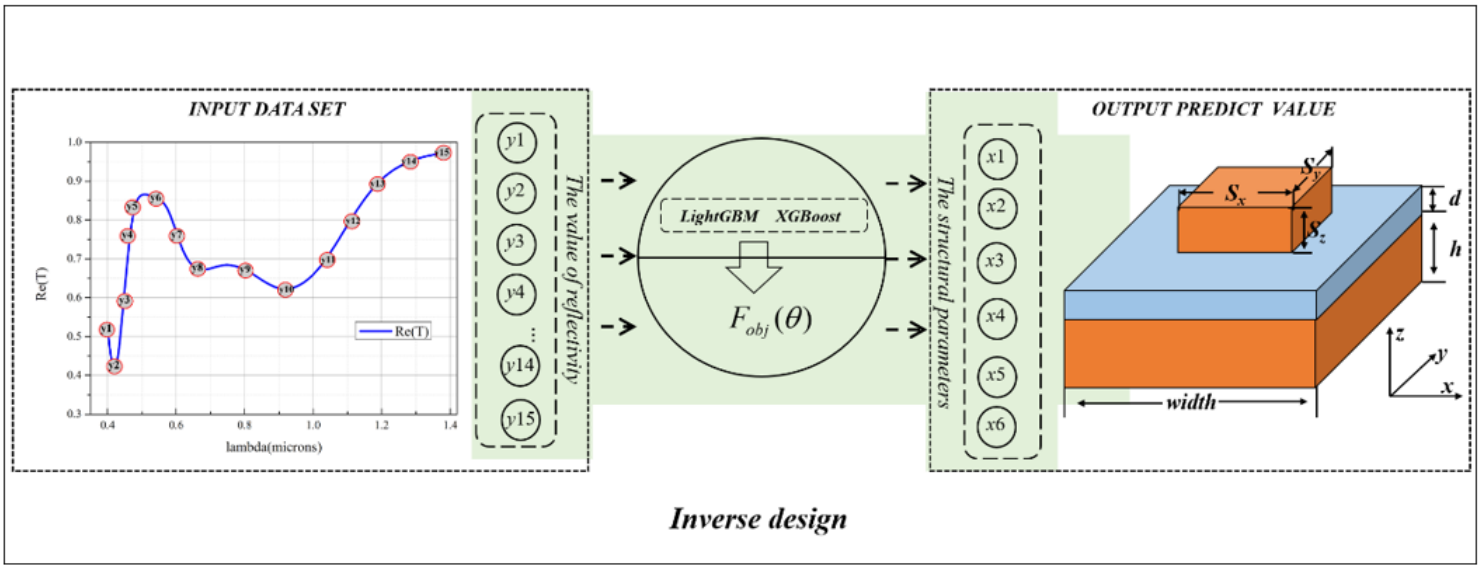

Figure 3

The process of predicting structural parameters by inverse design framework.

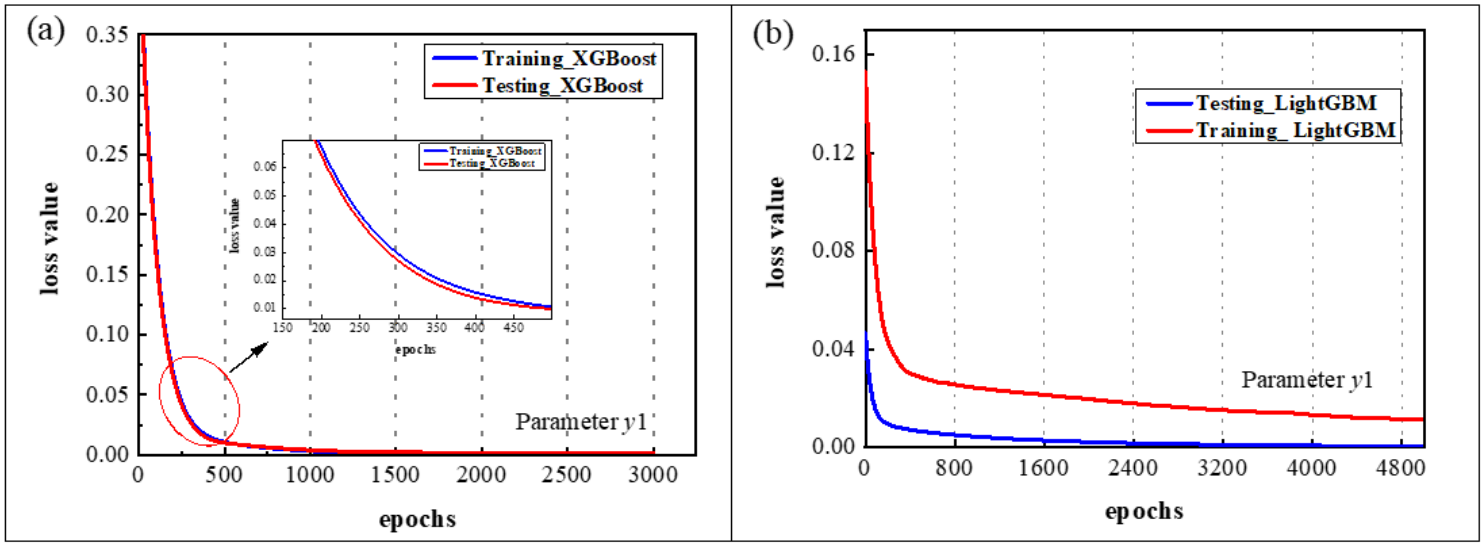

Figure 4

Model convergence of XGBoost and LightGBM (Parameter y1).

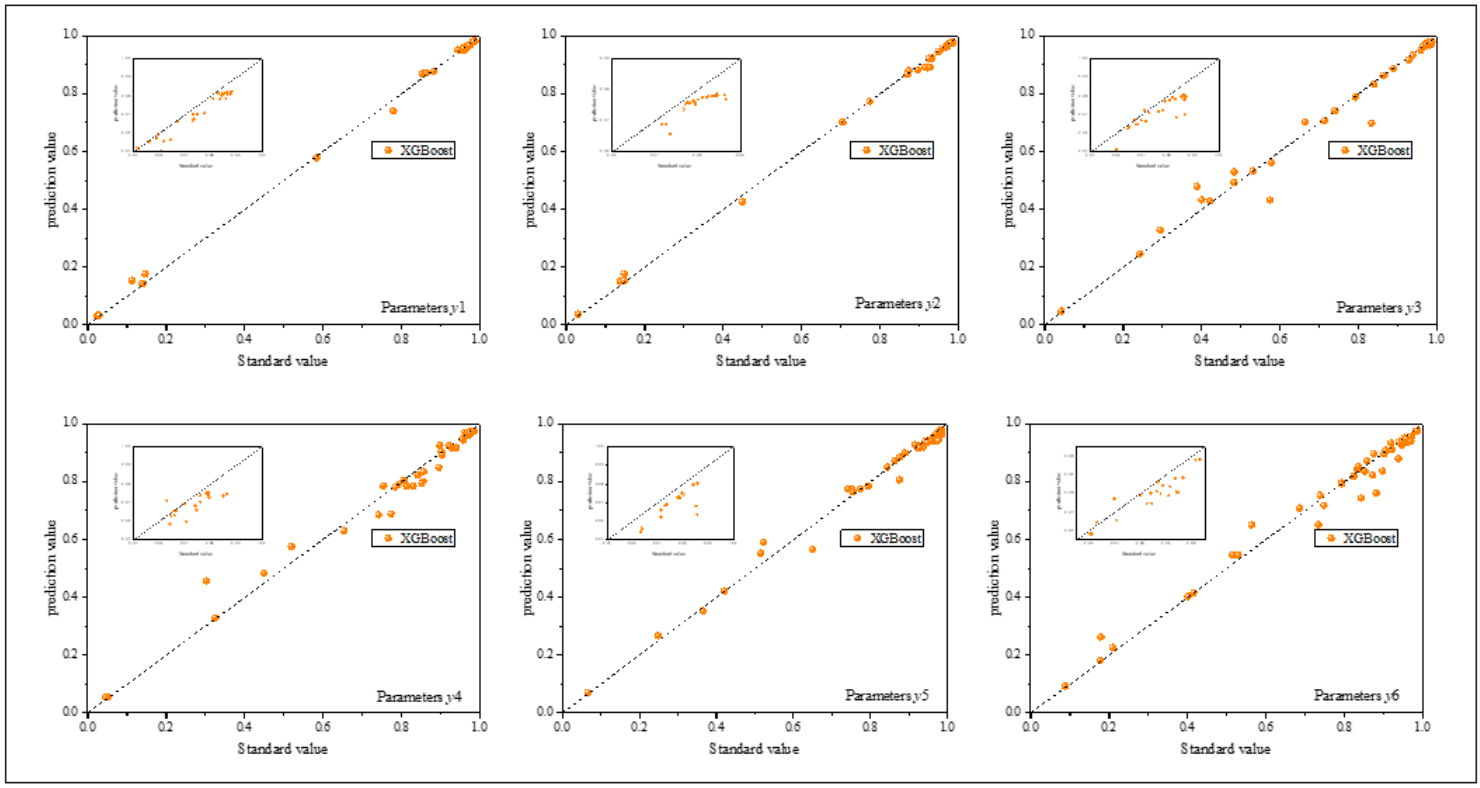

Figure 5

The distribution of predicted and true values in the test set (F-XGBoost).

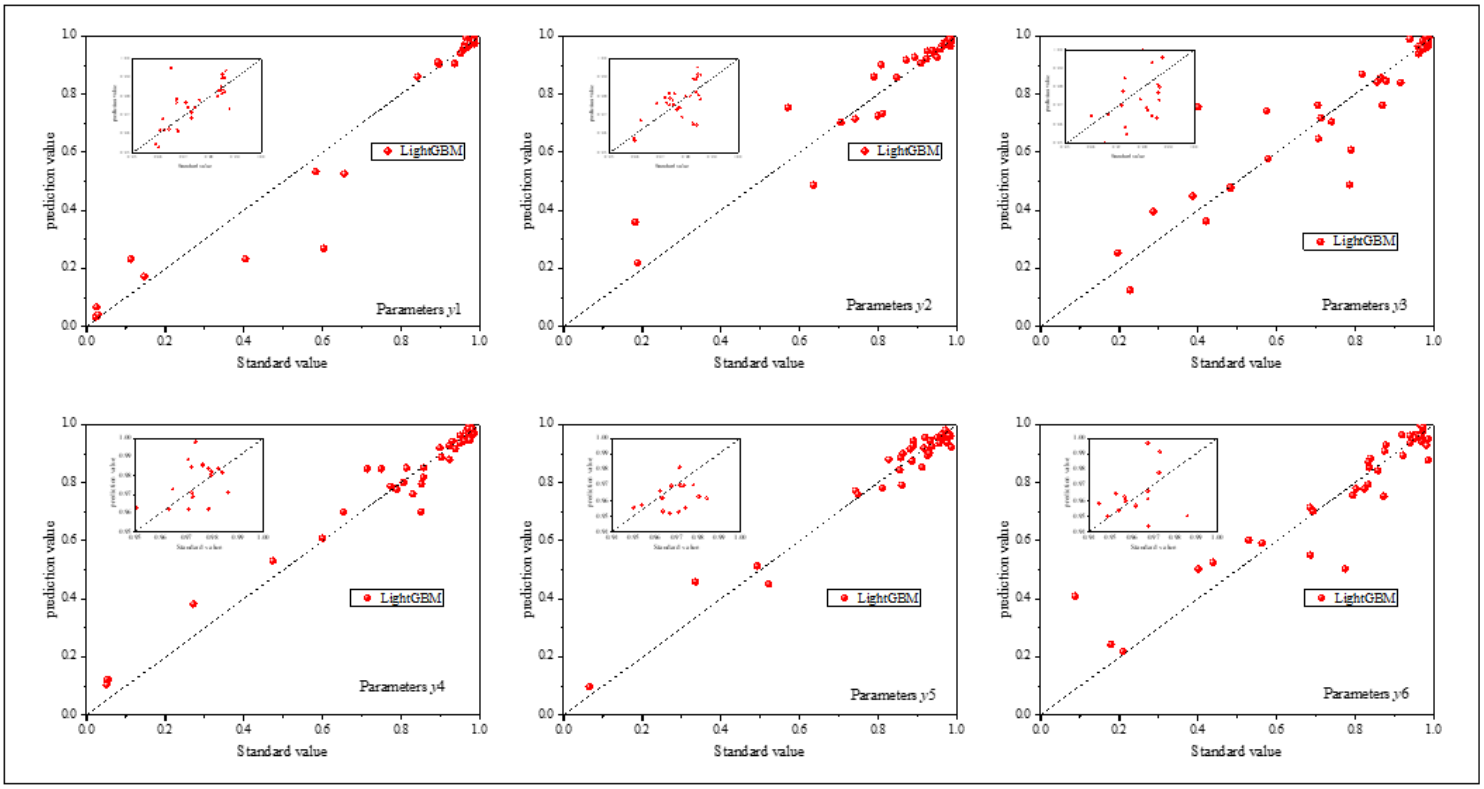

Figure 6

The distribution of predicted and true values in the test set (F-LightGBM).

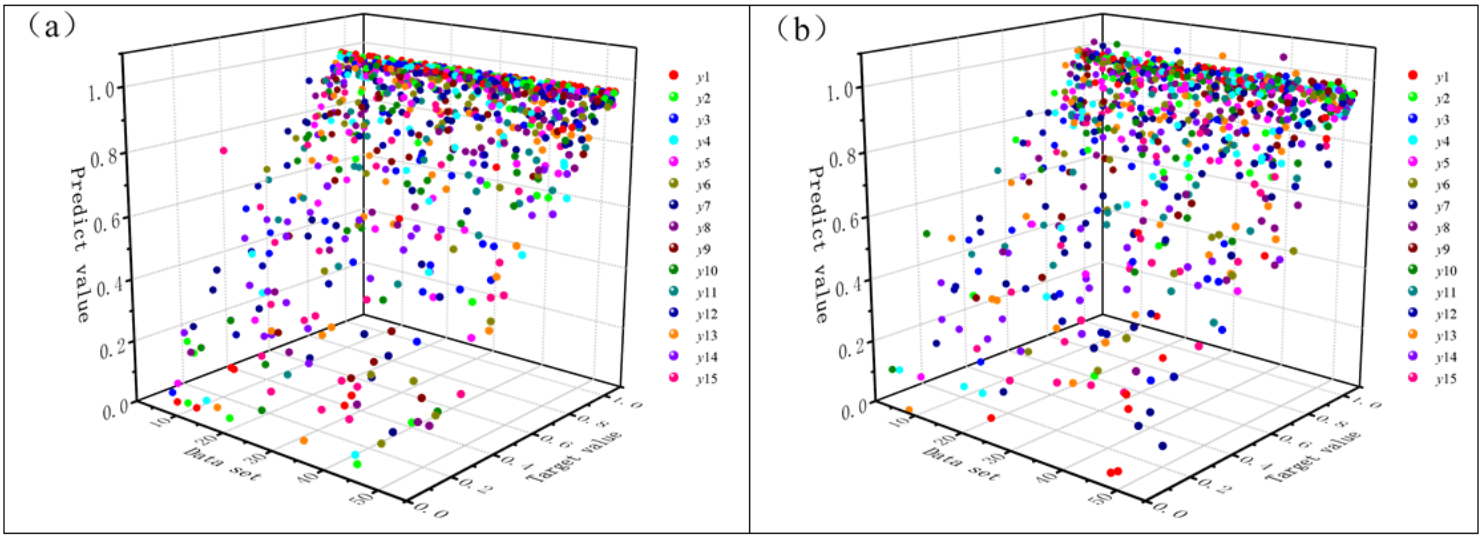

Figure 7

The distribution of the predicted value and target value of *y* refractive index in the test set

(a: F-XGBoost, b: F-LightGBM).

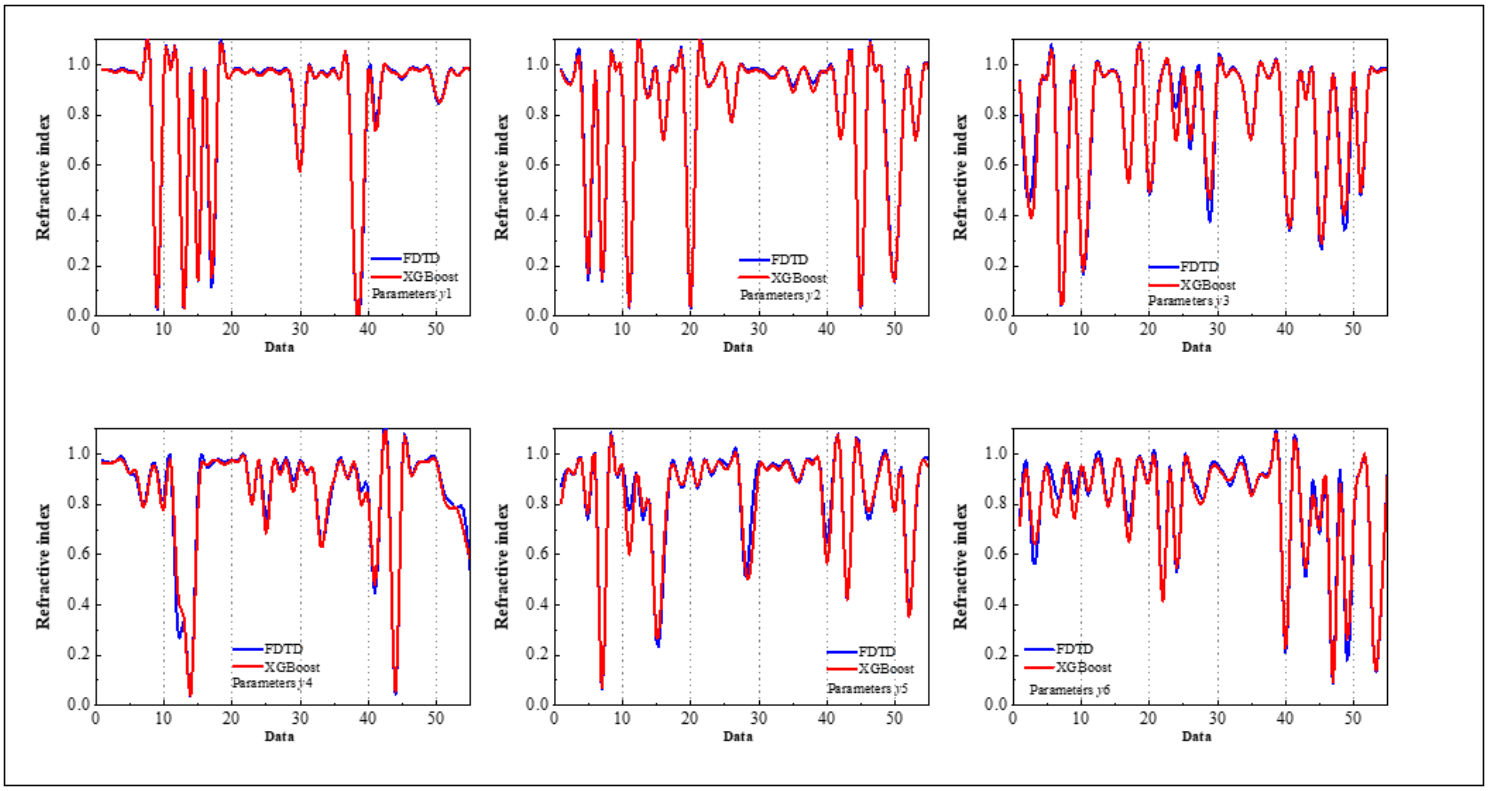

Figure 8

Curve of FDTD simulation value and model prediction value(F-XGBoost).

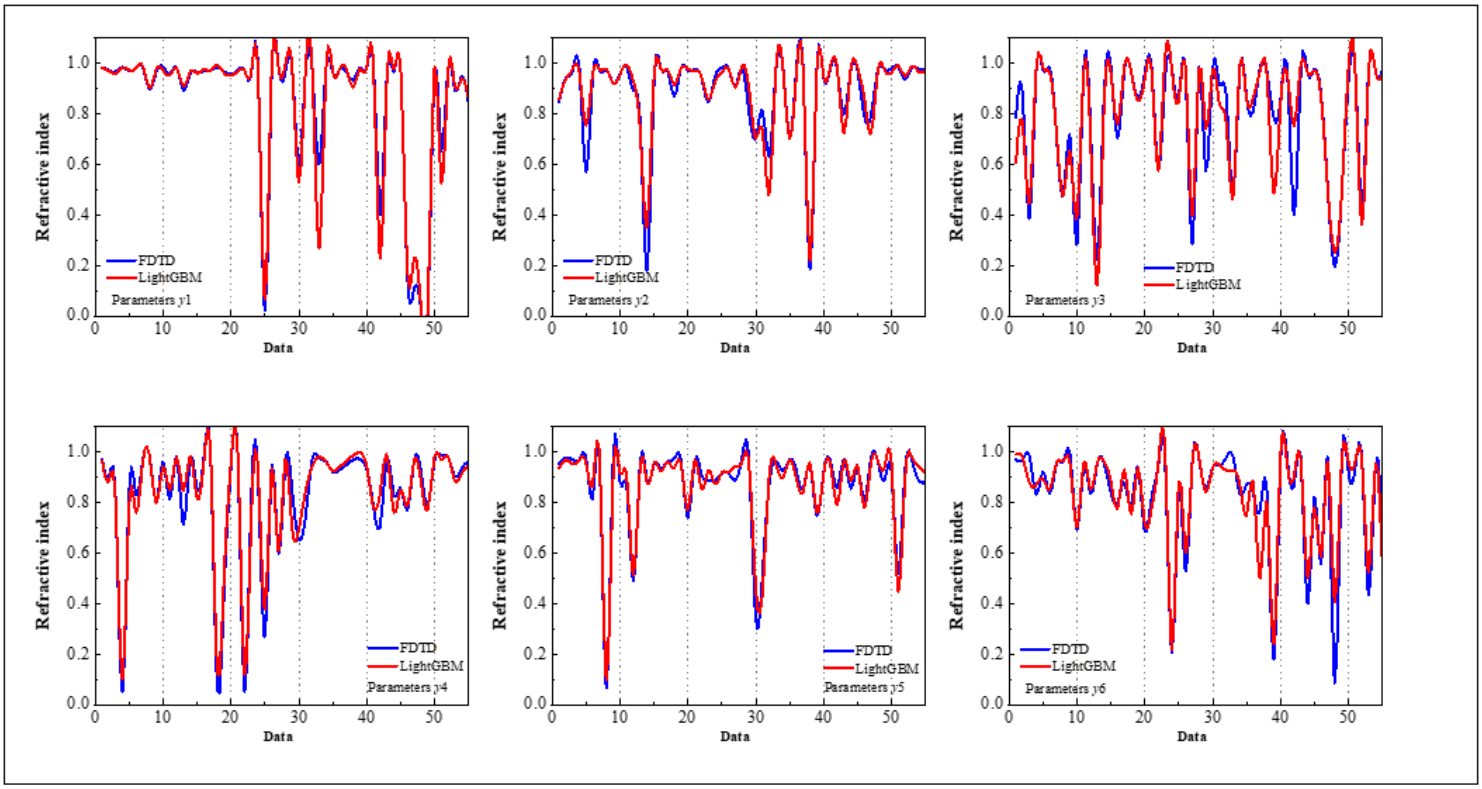

Figure 9

Curve of FDTD simulation value and model prediction value(F-LightGBM).

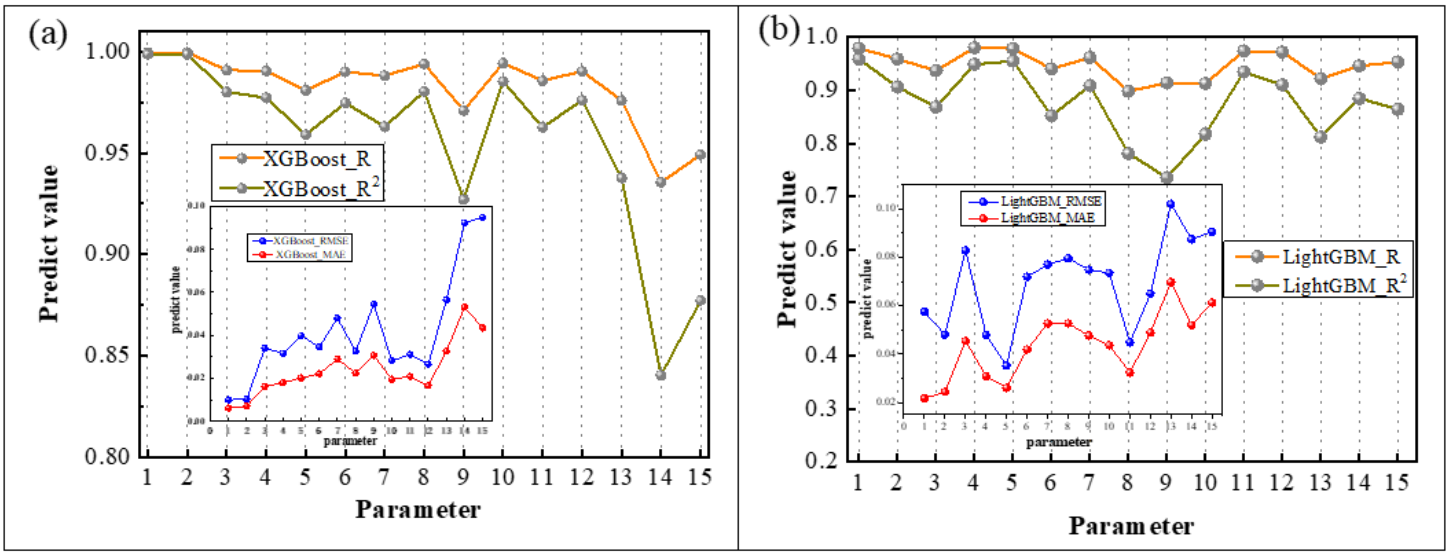

Figure 10

Model performance metrics (a: F-XGBoost, b: F-LightGBM).

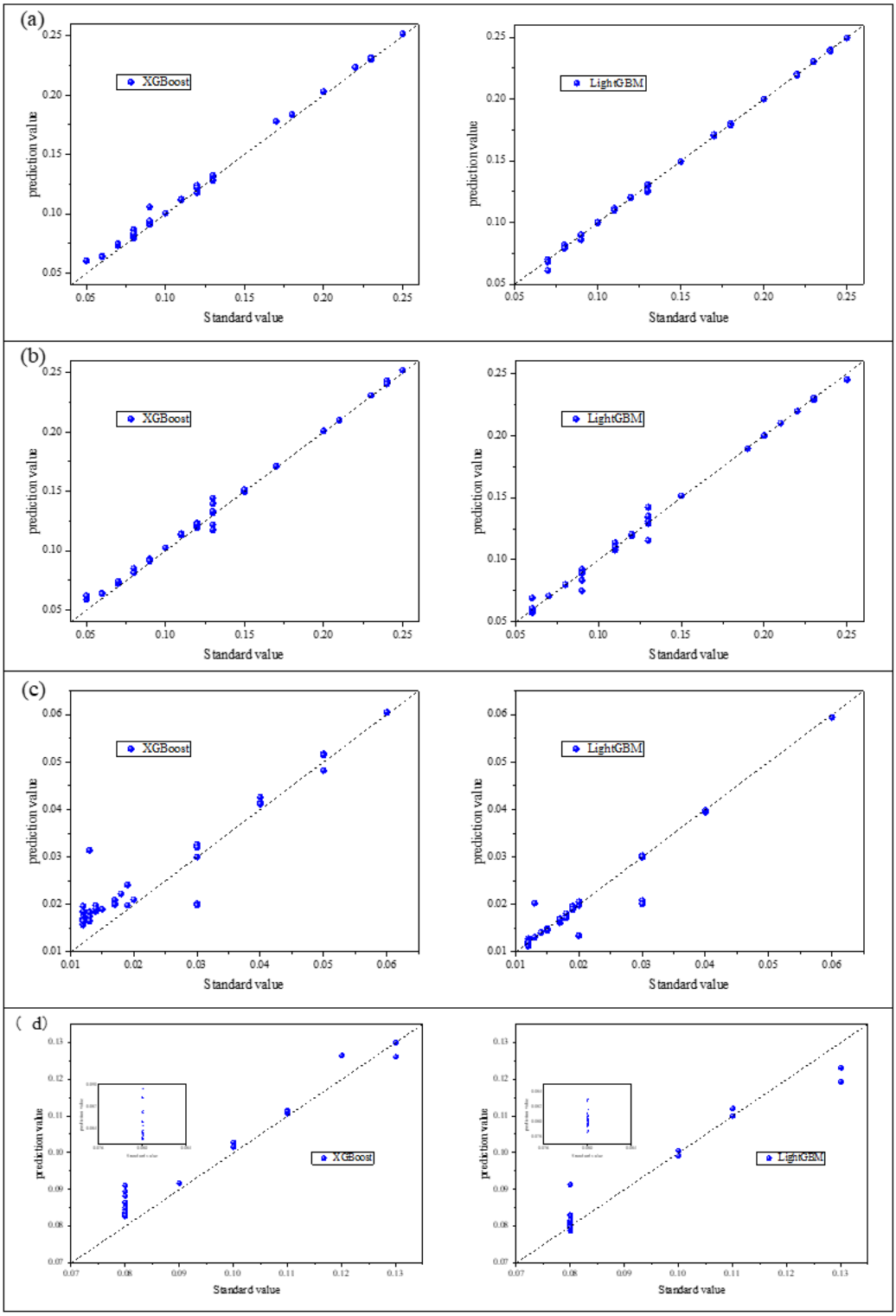

Figure 11

Distribution of predicted and true values in test data (I-XGBoost).

(a) parameters *x*1. (b) parameters *x*2. (c) parameters *x*3. (d) parameters *x*4

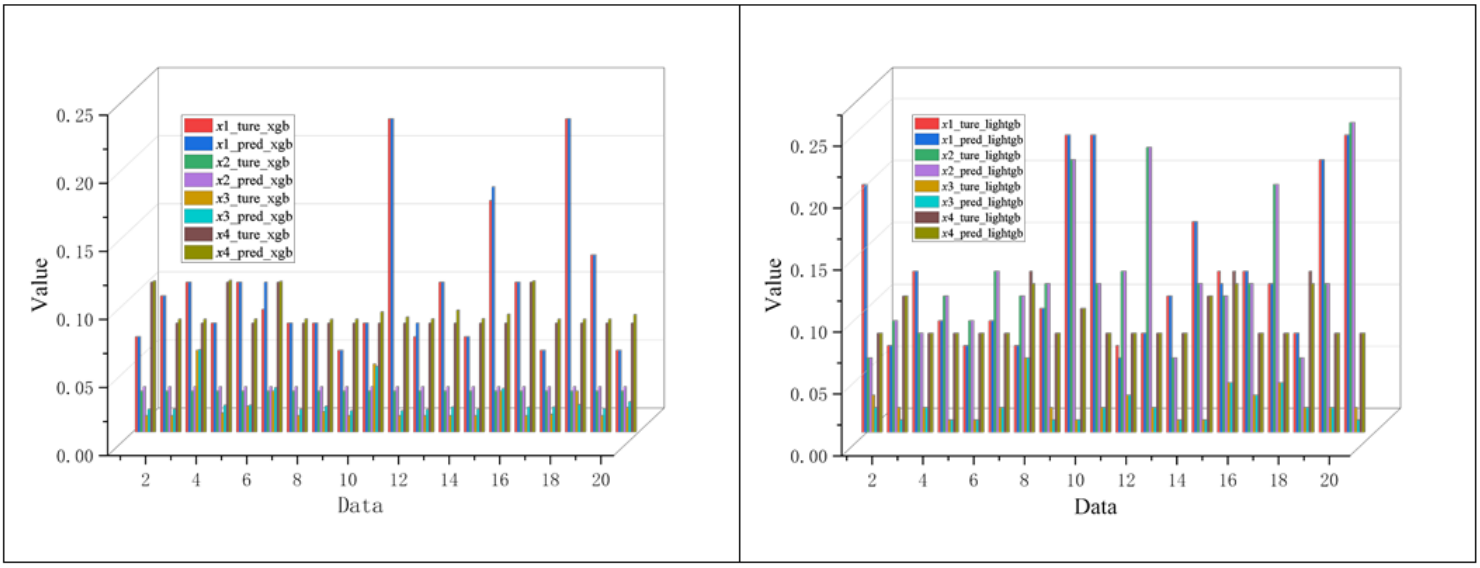

Figure 12

The predicted and target values of six structural parameters in inverse design

(I-LightGBM).

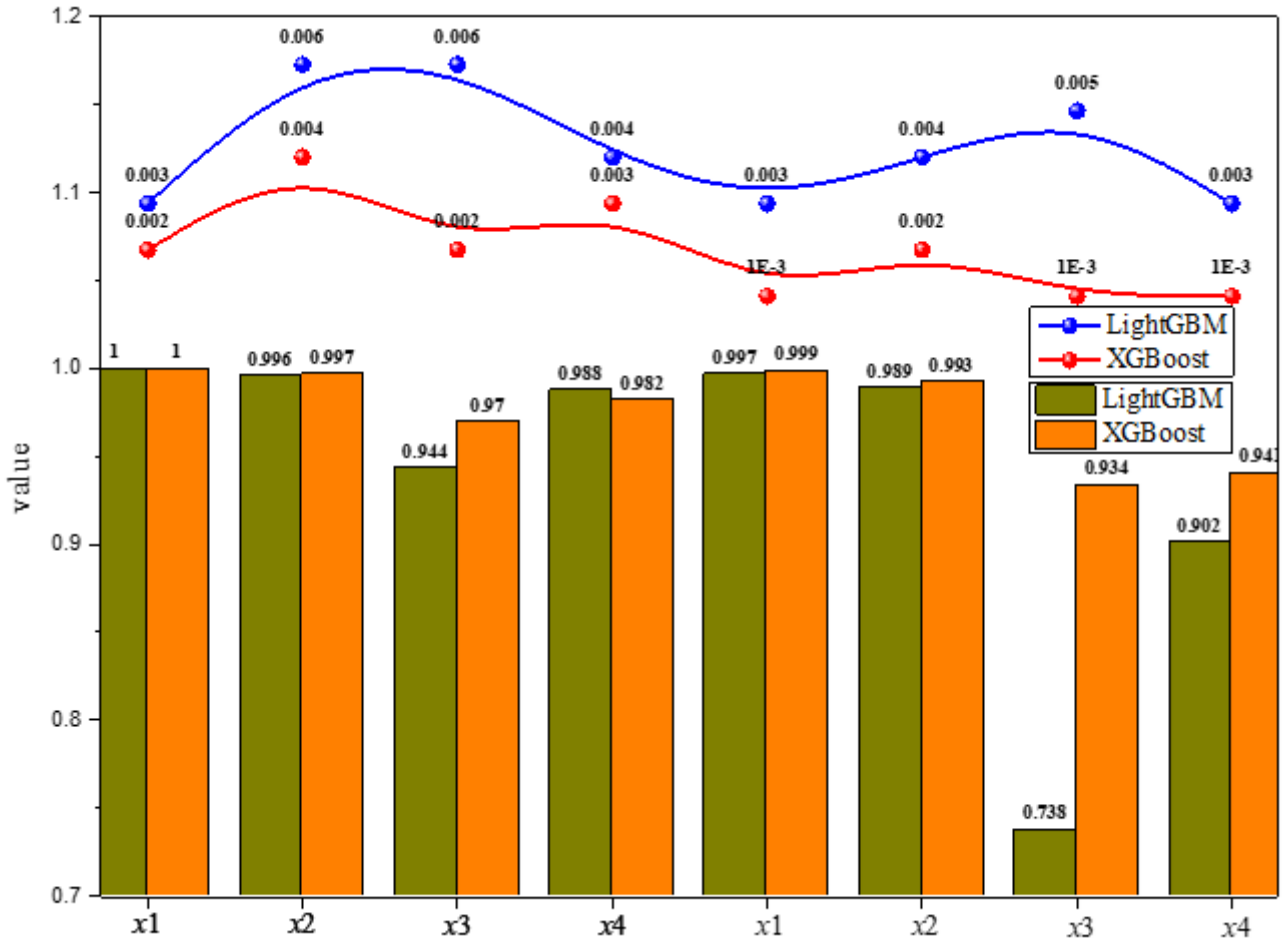

Figure 13

Comparison of XGBoost and LightGBM performance metrics.

(Lower left: R; Upper left: RMSE; Lower right: R^2; Upper right: MAE)

Supplementary Files

This is a list of supplementary files associated with this preprint. Click to download.

- Appendix.docx